Journal of Alloys and Compounds 509 (2011) 9406–9412

Contents lists available at ScienceDirect

Journal of Alloys and Compounds

journal homepage: www.elsevier.com/locate/jallcom

Electrodeposition and characterization of Ni–Co/SiC nanocomposite coatings

B. Bahadormanesh [a], A. Dolati [b,*], M.R. Ahmadi [a]

[a] Sharif University of Technology, Science and Engineering Department, Islamic Republic of Iran
[b] Sharif University of Technology, Materials Science and Engineering Department, Tehran, Islamic Republic of Iran

ARTICLE INFO

Article history:
Received 25 December 2010
Received in revised form 21 June 2011
Accepted 19 July 2011
Available online 26 July 2011

Keywords:
Coating materials
Metal matrix composites
Mechanical properties
Corrosion

ABSTRACT

Ni–Co/SiC nanocomposite coatings were electrodeposited in a modified watt type of Ni–Co bath containing 20 nm SiC particles to be codeposited. Potentiodynamic polarization tests were conducted to study the effect of the SiC particulates on the electrodeposition of Ni and Co. Scanning electron microscopy was used to assess the morphology of the Ni–Co alloy and Ni–Co/SiC nanocomposite coatings. The distribution of the particulates in the matrix was considered by means of transmission electron microscopy. Applying nanomechanical testing instruments coupled to atomic force microscopy, mechanical properties of the alloy and composite coatings were studied and compared. The presence of 11 vol.% SiC in the Ni–Co matrix increased hardness more than 60%. The average depth of scratch in the mentioned composite coating was about 15% less than that of the Ni–Co alloy coating. The corrosion penetration rate (CPR) of the Ni–Co alloy coating in a 3.5 wt.% NaCl solution was more than 17 times greater than that of the Ni–Co/SiC coating with 30.5 vol.% SiC.

1. Introduction

It is acknowledged that electrochemical embedding of finely dispersed rigid reinforcements in metallic matrices imparts exceptional advantages in terms of superior mechanical properties and better corrosion resistance as compared to pure metal and alloy coatings [1–11]. With the increasing availability of ever decreasing particle sizes, a large number of scholars have investigated to a greatest extent the electrocodeposition of micron, submicron and nano particles with metallic ions. The major challenge in this area seems to be the deposition of the high levels of non-agglomerated finely dispersed particles [12,13]. It has been reported that a reduction in particle size would improve microhardness, ameliorate wear and corrosion resistance [12–15]. The reduction of particle size decreases the codeposition content of the particles [12,13,16,17]; nevertheless, considering the number density of the particles in the coating, the rate of the nano particles codeposition is much higher than that of micro particles [12–14]. Garcia et al. [12,13] demonstrated the importance of the particle density instead of the volume percent of codeposited particles, especially when the characteristics of composite coatings containing particles of different sizes are compared, otherwise erroneous conclusions would be obtained. It has been revealed that micro-sized particles are codeposited at borders and edges of crystallites (inter-crystalline mechanism), while nano-sized particles are also incorporated inside crystals (intra-crystalline mechanism) [14].

In comparison with pure nickel, as a widespread engineering material, alloying of nickel with cobalt results in a higher hardness and superior wear and corrosion resistance at elevated temperatures. In addition, specific magnetic properties of nickel–cobalt alloys have made them a permanent candidate for recording head material in computer hard drive industries and micro-electrical mechanical systems [18–23]. These merits account for the widespread applications of this alloy as a metal matrix in electrocomposite coatings, where various particles have been incorporated in, through electrochemical methods, such as Cr_2O_3 [24], carbon nano tube (CNT) [25], yttria stabilized zirconia alumina (YZA) [26], SiC [27–29], Al_2O_3 [30,31], diamond [32], MoS_2 [33], $LaNi_5$ [34], barium ferrite [35], and Si_3N_4 [36]. To our knowledge, much work has not been reported on the electrochemical deposition of Ni–Co/SiC nanocomposite coatings. In the same authors' previous paper [37], Ni–Co/SiC electrodeposition process was modeled, and the kinetics aspects of the electrocodeposition were analyzed through the Guglielmi's model of codeposition. In addition, it was demonstrated that SiC nano particulate enhances the anomalous behavior of the Ni and Co electrodeposition, and the presence of these suspended particles in the deposition electrolyte increases the cobalt content of the deposits. Srivastava et al. [28,29] have reported that the wear resistance of Ni–Co/SiC composite coatings is superior to that of Ni/SiC composite coatings and the best wear resistance between the various compositions of Ni–Co/SiC coatings belongs to Co-rich composites.

* Corresponding author. Tel.: +98 21 6022721; fax: +98 21 6005717.
E-mail address: Dolati@Sharif.edu (A. Dolati).

0925-8388/$ – see front matter © 2011 Elsevier B.V. All rights reserved.
doi:10.1016/j.jallcom.2011.07.054

Table 1
Composition of the deposition electrolytes.

	$NiSO_4$	$NiCl_2$	$CoSO_4$	H_3BO_3	20 nm SiC	pH	T
Solution 1	220 g/dm^3	40 g/dm^3	20 g/dm^3	30 g/dm^3	0 g/l	4.2	50 °C
Solution 2	220 g/dm^3	40 g/dm^3	20 g/dm^3	30 g/dm^3	10 g/dm^3	4.2	50 °C
Solution 3	220 g/dm^3	40 g/dm^3	20 g/dm^3	30 g/dm^3	20 g/dm^3	4.2	50 °C
Solution 4	220 g/dm^3	40 g/dm^3	20 g/dm^3	30 g/dm^3	30 g/dm^3	4.2	50 °C
Solution 5	220 g/dm^3	40 g/dm^3	20 g/dm^3	30 g/dm^3	40 g/dm^3	4.2	50 °C
Solution 6	190 g/dm^3	20 g/dm^3	20 g/dm^3	30 g/dm^3	40 g/dm^3	4.2	50 °C
Solution 7	250 g/dm^3	60 g/dm^3	20 g/dm^3	30 g/l	40 g/dm^3	4.2	50 °C

This paper aims to investigate the electrodeposition and characteristics of this newly developed composite coating and to compare its properties with Ni–Co alloy coatings. To do end, Ni–Co alloy and Ni–Co/nano-SiC composite coatings were electrodeposited from a modified Watt type bath. The influence of bath electroactive species on the particles codeposition rate was analyzed. The surface morphology of the alloy and composite coatings as well as the quality of the SiC distribution in the Ni–Co matrix were studied. Mechanical properties of the composite coatings including nanohardness, nanoscratch resistance were compared with those of the alloy. Eventually, the corrosion resistance of the coatings in a 3.5% NaCl solution was investigated.

2. Experimental procedures

Table 1 lists the composition of the electrodeposition electrolyte of the coatings, which were based on the Watt's bath for the Ni–Co alloy deposition. Analytical reagents and triple distilled water were used for the solutions preparation. In order to prevent the agglomeration of the SiC particles, the electrolytes containing the particles were premixed and stirred by a magnetic stirrer (480 rpm) for 24 h and then by ultrasonic agitation (the power of 350 W and the frequency of 40 kHz) for 30 min just prior to the electrodeposition. 100 cm^3 beaker was used as the deposition bath and the volume of the electrolytes was 100 cm^3. Three vertical electrodes set-ups were employed for the codeposition process.

The electrochemical depositions were conducted by an IM6 model Zahner potentiostat/galvanostat controlled by the Thales software. A nickel plate (99.9% purity) was used as anode with the dimensions of 6 cm × 1 cm × 0.1 cm and up to 3 cm of its length was immersed in the electrolyte. The cathodes were copper plates with a size of 1 cm × 2 cm × 0.1 cm, mechanically polished to 2000-grit finish with SiC papers and chemically pre-treated by immersing in acetone for 15 min. The cathode plates were inserted in a PTFE holder with a 7 mm circular window exposed to the electrolyte. The deposition current densities were 1, 2 and 4 A/dm^2 and the coating thickness was 40 μm. Linear voltammetry with a 5 mV/s sweep rate was used to study the effect of the suspended SiC particles on the electrodeposition process. A scanning electron microscope (SEM, TESCAN model) was used to investigate the surface morphology of the coatings. The weight percentage of SiC in the coatings was determined using an Energy Dispersed X-ray micro-analyzer (EDX, Rontec model) coupled to SEM. The relative amount of Co and Ni in the deposited coatings was obtained based on the atomic absorption spectroscopy analysis (AAS, GBC model). The transmission electron microscopy TEM investigation of the composite coatings was performed using a ZEISS TEM model EM-10C operated at 100 kV to observe the distribution of the SiC particles in the Ni–Co matrix. Nanomechanical Test Instrument coupled to an atomic force microscope (AFM, Hysitron model) was also employed for nanohardness and nanoscratch tests.

The corrosion resistance of the deposited coatings was studied in a 3.5 wt.% NaCl solution by means of the polarization method. The measurements were performed at room temperature and in the non-stirred solution, where the applied sweep rate was 0.5 mV/s. The corrosion potential (E_{corr}), corrosion current density (I_{corr}) and corrosion penetration rate (CPR) were estimated and compared.

3. Results and discussion

3.1. Electrocodeposition of the SiC nano particulates with Ni and Co ions

Two of the main factors governing the particle content of layers are the current density and the particle concentration in the suspension. Fig. 1 is the correlation between the bath SiC concentration and the amount of SiC codeposited in the composite coatings for the three applied current densities. As seen, the amount of the codeposited SiC particles increases by increasing the bath

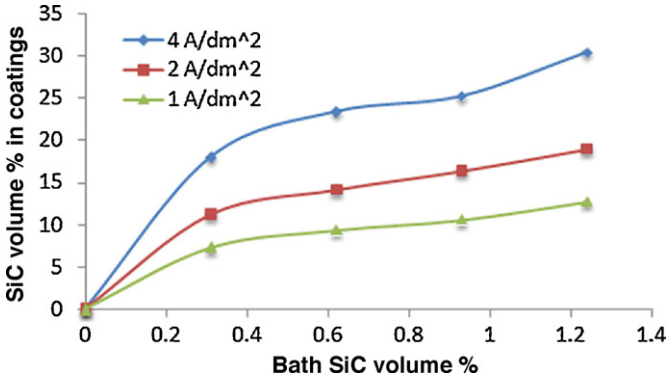

Fig. 1. Correlation between the bath SiC concentration and the amount of SiC codeposited in the composite coatings.

SiC concentration. This increasing trend is consistent with the Guglielmi's model of codeposition [37,38]. According to this model, the increase in the bath concentration of the particles increases the loose adsorption coverage of the particles on the cathode surface, where the higher percentage of the particles have a chance to transfer from the loose adsorption step to the strong adsorption step. Another point of the diagram is the increase in the codeposited SiC particles by increasing the applied current density. The increase in the applied current density provides a more reductive circumstance and enhances the chance of transfer from the loose adsorption step to the strong adsorption step. Thus, the increase of the current density increases the codeposition of the SiC particulates.

3.2. Role of the electroactive species concentration on the SiC codeposition

To study the effect of metallic ions as electroactive species in the electrolyte on the amount of the codeposited SiC particles, these particles were codeposited from the electrolytes with the different concentrations of Ni and Co ions. Solution numbers 5, 6, and 7 were used for this experiment. The electrodeposition was done

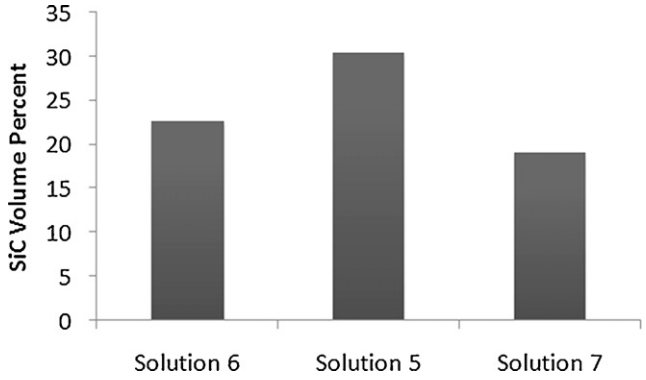

Fig. 2. Amount of SiC codeposited in the various deposition electrolyte concentrations.

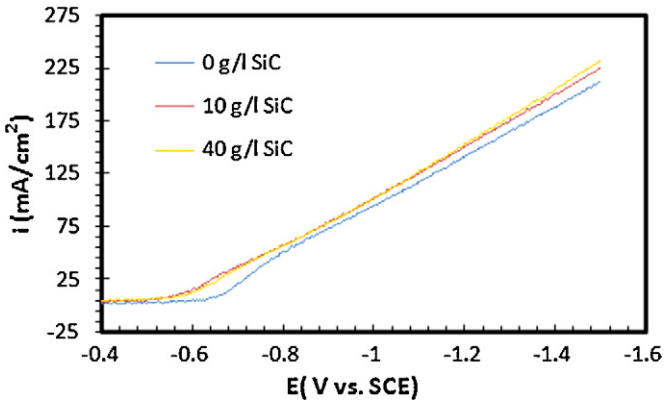

Fig. 3. Potentiodynamic polarization curves recorded on Cu in Ni–Co baths containing 0, 10 and 40 g dm^{-3} of SiC. Potential sweep rate 5 mV s^{-1}.

at a current density of 4 A/dm^2. The amount of codeposited SiC is shown in Fig. 2 for the three concentrations of nickel and cobalt sulfates in the bath. At first, the volume percent of the embedded SiC particles increases with increasing the ions concentration, but then decreases. This phenomenon is related to the mechanism of particles codeposition. According to the Guglielmi's model of codeposition, the particles are codeposited once the ions which are adsorbed on the particles surface are reduced. At the low concentration of the ions, insufficient metallic ions are adsorbed on the SiC nanoparticles and the higher percentages of the loosely adsorbed particles are desorbed from the cathode surface, resulting in a lower incorporation of the SiC particles. When the ions concentration increases, sufficient ions are present on the particles surface, which increases the strong adsorption and the incorporation of the particles. When the concentration exceeds the optimized value, the particles are saturated by the adsorbed ions, the competition between the freely solvated ions and the particles for the deposition is enhanced, and the rate of the freely solvated ions deposition increases, thereby falling the particles codeposition off [13,16,17,39].

3.3. Potentiodynamic polarization

Fig. 3 presents the potentiodynamic polarization curves of Solutions 1, 2 and 5 with the 5 mV/s potential sweep rate. The potential was swept in the cathodic direction from −0.3 V to −1.5 V versus the saturated calomel electrode (SCE). The little change in the slop of the curve around the potential of −0.6 V is related to the reduction of cobalt ions [18,41]. As the concentration of cobalt in this experiment is less than 0.1 M (0.071 M), this diffusion peak is anticipated. However, since the Ni ions concentration is high (0.983 M), the diffusion peak cannot be observed for Ni ions, and the Ni deposition is under charge transfer control. The point is related to the addition of the SiC nano particles to the deposition bath, which leads to the positive shift of Ni–Co polarization curve. Such behavior has been observed for conductive particles like Cr particles [42] and semi-conductive particles like SiC [43]. However, this positive shift is quite different with Shi et al.'s reports [27] for the SiC codeposition with nickel and cobalt ions. The positive shift is ascribed to an increase in the active cathode surface area and the increase in the ionic transfer by the SiC nano particulates, resulted from the fresh solution brought to the surface by the stationary film of liquid on each particle [42–45]. It will be discussed in the next section by SEM where the presence of the SiC particulates in growing Ni–Co matrix increases the effective surface area of the cathode. In other words, under the identical deposition potential, the effective surface area of Ni–Co/SiC is more than that of the Ni–Co deposits. Another contributing factor in the positive shift of the polarization curve in the presence of the SiC nano particulates is the fact that the SiC nanoparticles can enhance the adsorption of the ions (especially Co^{2+}) and consequently increase the current density [28,37,30,31].

3.4. Surface morphology and distribution of the particles

Fig. 4 compares the surface morphology of the Ni–Co alloy and the Ni–Co/SiC composite coatings deposited in Solutions 1 and 5 at the current density of 4 A/dm^2. The Co content of the alloy coating (Fig. 4a) is about 33 at.%, obtained by the AAS analysis. It is seen that the mentioned alloy exhibits a dense irregular spherical morphology. Fig. 4b is the surface morphology of the Ni–Co/SiC composite coating. The incorporation of the nano SiC particles has changed the morphology to cauliflower-like, where the cobalt content is about 38%. Fig. 4c shows the protrusions of the composite coating in a higher magnification. The EDX analysis shows that these cauliflower-like protrusions are fresh deposits enriched with the SiC nanoparticles, while in the other areas the codeposited SiC nanoparticles were engulfed by Ni–Co deposits. Due to the small dimensions, low density, and low adsorption of electrons, it was difficult to distinguish the particles from the Ni–Co matrix using SEM. Moreover, they are coated by ions in the bath, and they are engulfed by these reduced ions during the deposition. The TEM image of the deposited composite coating is presented in Fig. 4d. The relative uniform distribution of the SiC particles can be observed in the TEM image, demonstrating that the employed method for the dispersion and deagglomeration of the SiC nanoparticle is effective and successful.

3.5. Nanomechanical properties

In order to determine nanomechanical properties, a Berkovich indenter was used to study the nanohardness and nanoscratch resistance of the electrodeposited alloy and composite layers. The instrument of nanoindentation test is capable of performing very precise hardness and scratch test by providing real-time load–displacement data while the indentation is in progress. The instrument provides high spatial images from the indentation impressions and enables the operator for quantitative rugosimetery (surface roughness analysis).

A Berkovich indenter is a nano indenter used for testing the hardness of a material. The Berkovich tip has the same projected area to depth ratio as a Vickers indenter.

Firstly, it is worth to mention that in the case of Ni–Co/30.5% SiC (the composite with the highest amount of incorporated SiC), due to the high surface roughness, the hardness values and scratch resistance data measured by the nano-indenter were scattered and unreliable. In addition, the AFM image of the mentioned composite was not clear. Therefore, the nanoscratch test on the composite with the highest amount of the incorporated particles was impossible. Instead, a composite with the lower amount of SiC, Ni–Co/11% SiC prepared from Solution 2 electrodeposited at the current density of 2 A/dm^2, was chosen to compare the hardness and scratch resistance of the composite and alloy coated samples.

Fig. 5 presents the AFM images of the residual diagonal impressions of the hardness test. The nanohardness test results are based on the area function determined after indentation to take into account the blunting of the indenter tip during the penetration into the specimen.

A triangular indentation is clearly seen in the AFM micrographs. The residual impression shown in the images can be explained by a slight amount of piling-up of the material around the sides of the indenter. The additional pile-ups around the indentation give an evidence of the plastic behavior of the coatings [46,47]. It is seen that the amount of plastic deformation in the case of the alloy is much more than the composite coating, which demonstrates the

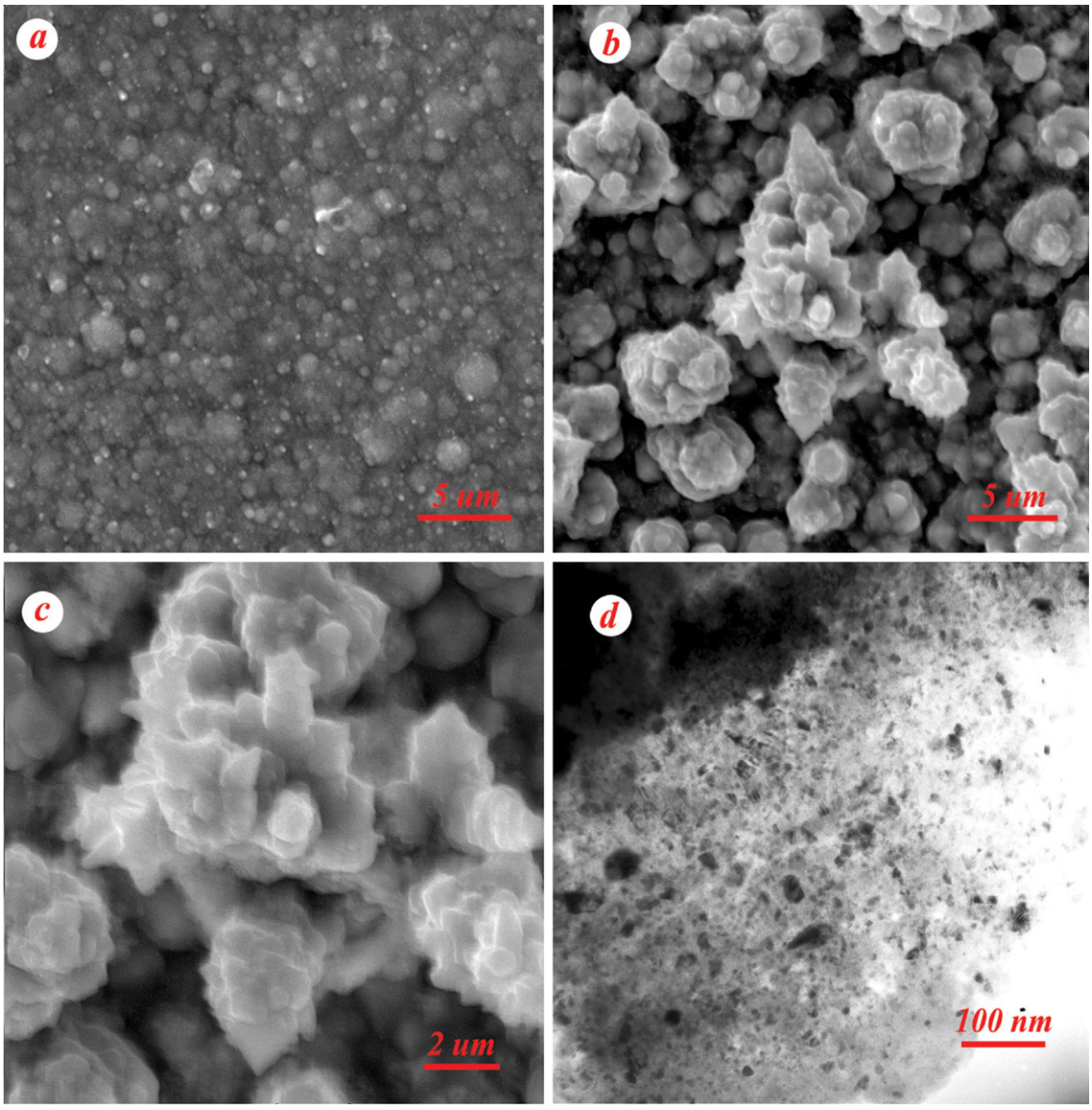

Fig. 4. Surface morphology of the (a) Ni–Co alloy coating, (b) Ni–Co/SiC composite coating, and (c) Ni–Co/SiC in a higher magnification; (d) TEM image of the Ni–Co/SiC composite coating.

lower hardness of the alloy coating in comparison to the composite one. This process can be caused by the motion of matrix crystals' grain boundaries and/or the generation of cracks. The incorporation of the nano SiC particulates increases the hardness value more than 60% from 2.1 GPa to 3.43 GPa. It is anticipated that the hardness of the composites with a higher amount of SiC would be more than this value.

It is known that the hardness of metal matrix composites depends on many factors such as: (i) the amount of particles, (ii) the size of dispersed phases, (iii) inter-particle spacing, (iv) the distribution of particles, (v) the morphology of particles, (vi) the structure and mechanical characteristics of the matrix, and (vii) particles' interfaces [12,13,40,48,49]. The amount and size of particles represent two types of reinforcing mechanisms in metal matrix composite materials, namely dispersion-strengthening and particle-strengthening. In the case of the dispersion-strengthening mechanism, the matrix carries the load and the fine particles impede the motion of dislocations. Strengthening is achieved because the particles restrain the matrix deformation by a nanomechanical constraint. However, in the case of the particle-strengthening mechanism, the load is carried by both the matrix and particles. Thus, in the Ni–Co/nano SiC coating, the increase in hardness can be attributed to a dispersion-strengthening effect [12–14,40,48,49]. It should be noticed that, to obtain a dispersion-strengthening effect, it is crucial to achieve a uniform embedding of non-agglomerated particles in the matrix [12–14,48]. As demonstrated by the TEM image, the non-agglomerated SiC nano particulates have been uniformly distributed in the metallic matrix.

To study the tribological performance of the electrodeposited composite coatings, the scratch test was carried out by the AFM/LFM (Lateral Force Microscopy) technique. Fig. 6 displays the normal force and lateral displacement of the indenter (i.e. respectively, the applied force and the amount of indenter displacement on the surface) vs. the scratch testing time, controlled automatically by the instrument. In the AFM/LFM measurements, the lateral force between the sample surface and the cantilever tip (the force applied to the indenter tip by the coating) is mainly composed of the adhesive and cantilever bending forces. Fig. 7 shows the lateral force or frictional force as a function of the loading time. The frictional force can be related to the shear strength of the contacting points. Fig. 8 reveals the rugosimetric profiles (surface roughness profile)

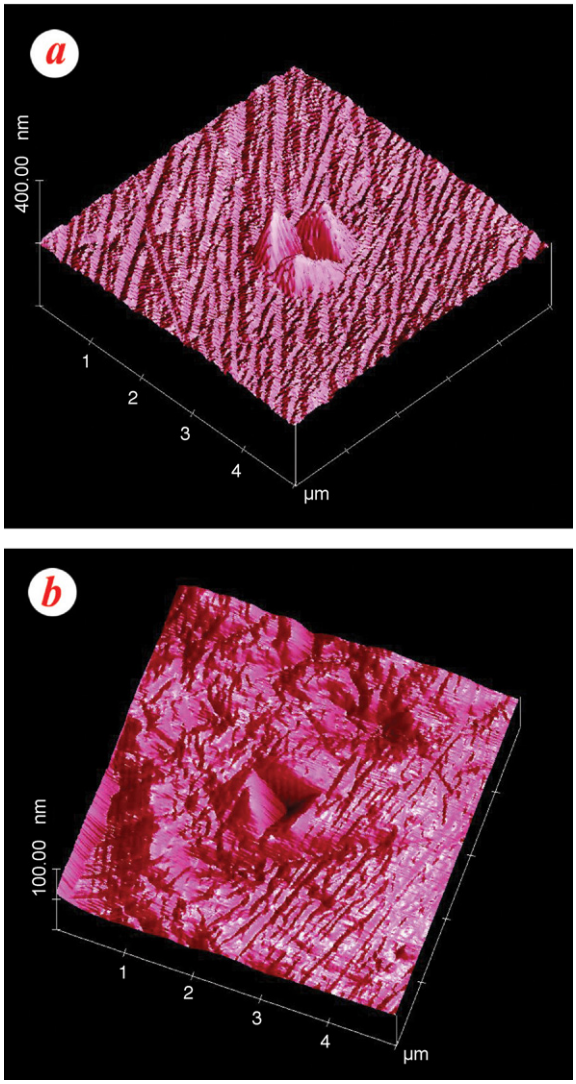

Fig. 5. AFM scans of the hardness test residual impressions on the Ni–Co alloy and Ni–Co/SiC composite coatings.

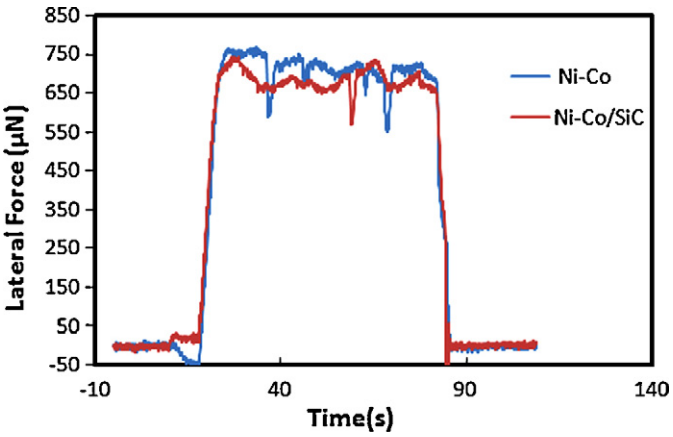

Fig. 7. Frictional force as a function of the loading time during the scratch test.

of the alloy and composite coating surfaces after the scratch test. Similar to the hardness test, the pill-up of the material around the indenter impressions sides is indicative of plastic deformation. In the case of the composite coating, plastic deformation and generally the depth of scratch is less. Fig. 9 shows the normal displacement of the Berkovich indenter into the coatings as the function of loading time. As is evident, the average depth of scratch in the case of the composite coating is about 15% less than that of the Ni–Co alloy. This behavior is consistent with the hardness test results and demonstrates the superior scratch resistance of the composite coating in comparison to the alloy one. After the measurements of the surface profile of the frictional force deposits, no breakage, cracks or detachments are observed.

The mentioned reasons for the higher hardness of the composite can be considered as the causes of the better scratch resistance of the composite coating. The scratch profiles observed in the tip track after the tests suggest that debris and pulled-out SiC particles have an adverse effect when they remain in the sliding contact area. A competition takes place between the beneficial increase in hardness due to the reinforcing SiC particles codeposited in the Ni–Co electrodeposits and their adverse lateral effect.

3.6. Corrosion resistance

Fig. 10 compares the polarization curve of the coatings deposited in solutions 1 and 2 and 5 at the current density of 4 A/dm^2. The prepared coatings contain respectively 0, 18 and 30.5 volume per-

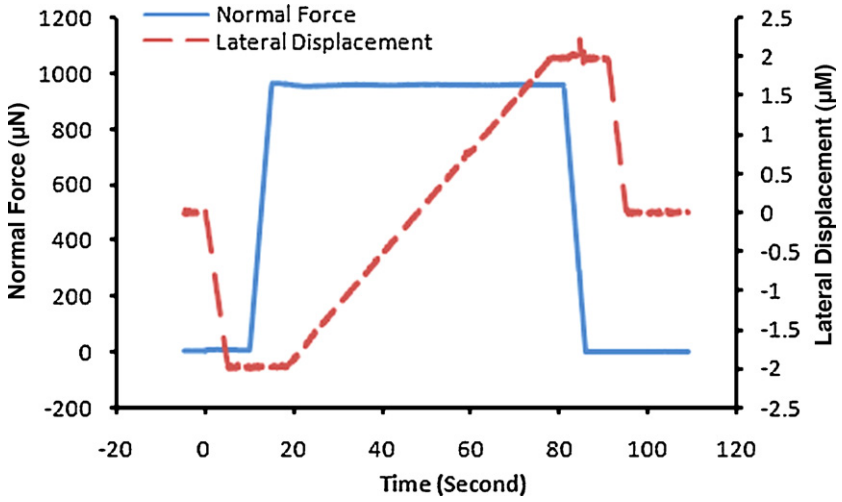

Fig. 6. Normal force and lateral displacement vs. testing time.

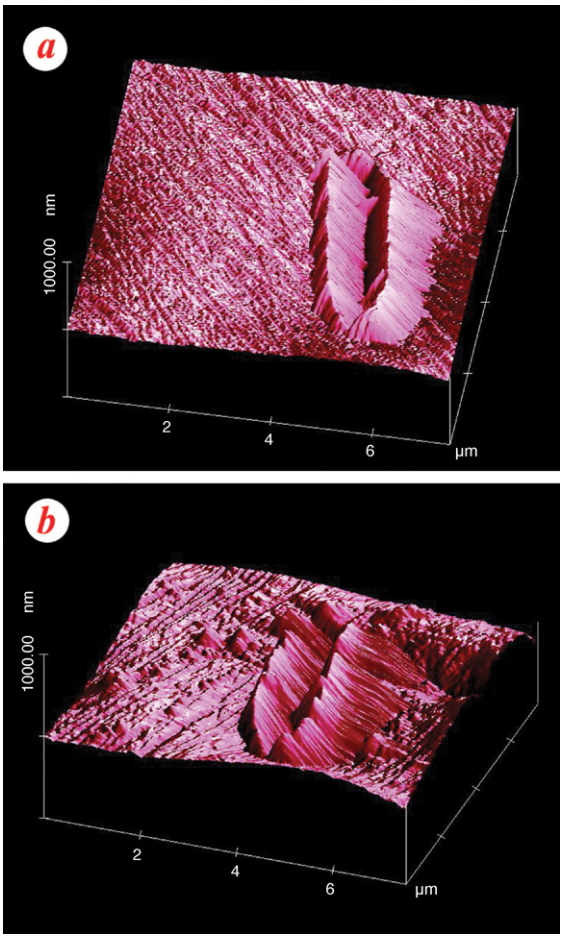

Fig. 8. AFM scans of the three-dimensional rugosimetric profiles after the scratch tests: (a) Ni–Co alloy and (b) Ni–Co/SiC composite coatings.

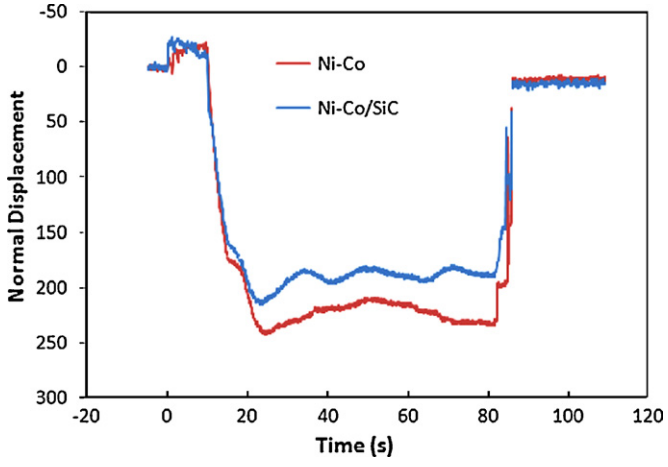

Fig. 9. Normal displacement vs. loading time diagrams of the scratch tests for the Ni–Co and Ni–Co/SiC coatings.

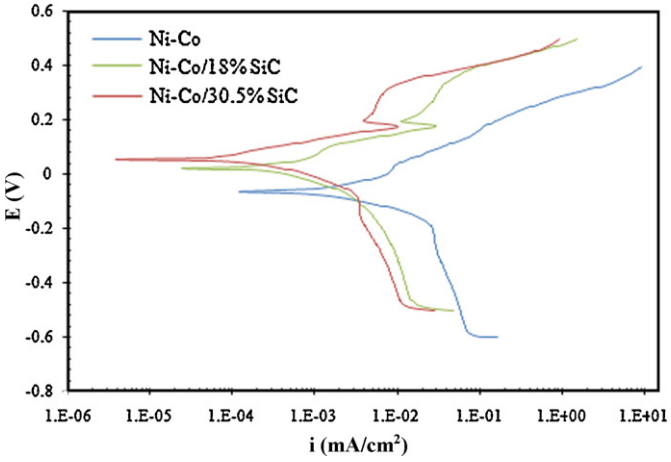

Fig. 10. Anodic polarization curves recorded in 3.5 wt.% NaCl solution for the Ni–Co and Ni–Co/SiC coatings (potential sweep rate 0.5 mV s^{-1}).

cent SiC nano particulates. The corrosion data extracted from the polarization curves are summarized in Table 2.

A positive shift of E_{corr} values was observed for the composite coating samples, indicating their better corrosion resistance in comparison to the alloy one. Moreover, the corrosion current density of the composite coatings is much less than that of the alloy one. Although Ni and Co are able to be in a passive state, as a chlorine ion-containing medium was employed, passivation would not happen. Nevertheless, contrary to our anticipation, a polarized area is observed around potential of +0.15 V for the composite coatings.

Assuming the non-selective and non-localized corrosion of the elemental constituents of the alloy and composite coatings, the corrosion penetration rate (CPR) of the samples was calculated in terms of μm/year and summarized in Table 2. In order to calculate CPR of the coatings accurately, the reduction of the surface area for dissolution by the SiC particulates was considered and subtracted from the overall surface area, and after the calculation of the corrosion current density based on new surface areas, these current densities were converted to the corrosion penetration rate. However, CPR of Ni–Co/18% SiC and Ni–Co/30.5% SiC was respectively more than 2 and 17 times less than that of the Ni–Co alloy coating. Apart from the structural modification of the matrix crystallites expressed through the alteration of the preferred orientation [50,51], it seems that the intrinsic corrosion resistant nano SiC particles could act as inert physical barriers and hinder the initiation and development of corrosion defects, which improves the overall corrosion resistance of the composite coatings especially in the high volume fractions of the reinforcements. Another point is the fact that, in the case of the composite coatings, the nano particles embedded at the borders of the matrix crystallites, as well as inside the matrix crystals and this mechanism of embedment can help to prevent pits from growing up. These might be the reason of the polarization area around potential of 0.15 V for the composite coatings. The alteration of the corrosion resistance cannot only be attributed to the incorporation of the SiC nano particles, since the incorporation of the SiC nano particles alters the ratio of Co to Ni in the deposits. By increasing the amount of SiC, the Co to Ni ratio increases [37]. An experiment [22] has showed that in 3.5 wt.%

Table 2
Corrosion data extracted from the polarization curves.

	E_{corr} (mV)	I_{corr} (mA/cm^2)	CPR (μm/year)
Ni–Co	−67	2×10^{-4}	2.160
Ni–Co/18% SiC	+23	7×10^{-5}	0.808
Ni–Co/30.5% SiC	+53	10^{-5}	0.122

NaCl, the corrosion resistance of an electrodeposited Ni coating is better than that of Co coating, and among Ni–Co coatings with the various amounts of Co content, Ni–20%Co alloy with a FCC structure has the best corrosion resistance. The higher amounts of the Co content led to a lower corrosion resistance. Hence, it seems that in the Ni–Co/SiC nanocomposite coatings, although the general corrosion resistance of the composite coatings is better than alloy one, due to the higher amount of Co content the corrosion resistance of the matrix is worse than the alloy coating.

4. Conclusions

1. Ni–Co/SiC composite coatings were deposited in a modified Watt type bath with the maximum particles content of 30.5 vol.%. Employing a method, comprising the magnetic stirring and the ultrasonic agitation (the power of 350 W and the frequency of 40 kHz) of the nano SiC suspension, was effective for the deagglomeration of the mentioned particulates. The non-agglomerated finely dispersed nano SiC particulates were uniformly distributed in the Ni–Co matrix.
2. The incorporation of the SiC particles altered the surface morphology of Ni–Co from dense irregular to cauliflower-like for Ni–Co/SiC.
3. In the electroactive species concentrations higher and lower than the optimized value, the amount of codeposited SiC levels off. This phenomenon in the lower concentrations was attributed to the lack of enough ions for the particles strong adsorption, and in the higher concentrations, it was attributed to the successful competition of freely solvated ions with the particles for the codeposition.
4. The addition of the SiC nano particles to the deposition bath led to the positive shift of the Ni–Co polarization curve.
5. The presence of 11 vol.% SiC in the Ni–Co matrix increased hardness more than 60%, i.e. from 2.1 GPa to 3.43 GPa. The average depth of scratch for the mentioned composite coating was about 15% less than that of the Ni–Co coating.
6. The corrosion penetration rate (CPR) of the Ni–Co/SiC coating with 30.5 vol.% SiC was more than 17 times smaller than that of the Ni–Co alloy in a 3.5 wt.% NaCl solution.

References

[1] S.T. Aruna, V.K. William Grips, K.S. Rajam, J. Alloys Compd. 468 (2009) 546–552.
[2] Q. Li, X. Yang, L. Zhang, J. Wang, B. Chen, J. Alloys Compd. 482 (2009) 339–344.
[3] J. Panek, A. Budniok, Surf. Coat. Technol. 201 (2007) 6478–6483.
[4] L. Benea, F. Wenger, P. Ponthiaux, J.P. Celis, Wear 266 (2009) 398–405.
[5] A. Zoikis-Karathanasis, E.A. Pavlatou, N. Spyrellis, J. Alloys Compd. 494 (2010) 396–403.
[6] H. Ataee-Esfahani, M.R. Vaezi, L. Nikzad, B. Yazdani, S.K. Sadrnezhaad, J. Alloys Compd. 484 (2009) 540–544.
[7] A.A. Aal, H.A. Gobran, F. Muecklich, J. Alloys Compd. 473 (2009) 250–254.
[8] B.M. Praveen, T.V. Venkatesha, J. Alloys Compd. 482 (2009) 53–57.
[9] A. Sohrabi, A. Dolati, M. Ghorbani, A. Monfared, P. Stroeve, Mater. Chem. Phys. 121 (2010) 497–505.
[10] C. Wang, Y. Zhong, J. Wang, Z. Wang, W. Ren, Z. Lei, Z. Ren, J. Electroanal. Chem. 630 (2009) 42–48.
[11] F.F. Xia, C. Liu, F. Wang, M.H. Wu, J.D. Wang, H.L. Fu, J.X. Wang, J. Alloys Compd. 490 (2010) 431–435.
[12] I. Garcia, A. Conde, G. Langelaan, J. Fransaer, J.P. Celis, Corros. Sci. 45 (2003) 1173–1189.
[13] I. Garcia, J. Fransaer, J.-P. Celis, Surf. Coat. Technol. 148 (2001) 171–178.
[14] E.A. Pavlatou, M. Stroumbouli, P. Gyftou, N. Spyrellis, J. Appl. Electrochem. 36 (2006) 385–394.
[15] K.H. Hou, M.D. Ger, L.M. Wang, S.T. Ke, Wear 253 (2002) 994–1003.
[16] H.-K. Lee, H.-Y. Lee, J.-M. Jeon, Surf. Coat. Technol. 201 (2007) 4711–4717.
[17] S.K. Kim, H.J. Yoo, Surf. Coat. Technol. 108–109 (1998) 564–569.
[18] A. Dolati, M. Sababi, E. Nouri, M. Ghorbani, Mater. Chem. Phys. 102 (2007) 118–124.
[19] G.D. Hibbard, K.T. Aust, U. Erb, Mater. Sci. Eng. A 433 (2006) 195–202.
[20] L. Wang, Y. Gao, Q. Xue, H. Liu, T. Xu, Appl. Surf. Sci. 242 (2005) 326–332.
[21] L.M. Chang, M.Z. An, S.Y. Shi, Mater. Chem. Phys. 94 (2005) 125–130.
[22] M. Srivastava, V.E. Selvi, V.K.W. Grips, K.S. Rajam, Surf. Coat. Technol. 201 (2006) 3051–3060.
[23] K.R. Marikkannu, G.P. Kalaignan, T. Vasudevan, J. Alloys Compd. 438 (2007) 332–336.
[24] K. Kumar, R. Chandramohana, D. Kalyanaraman, Appl. Surf. Sci. 227 (2004) 383–386.
[25] L. Shi, C.F. Sun, P. Gao, F. Zhou, W.M. Liu, Surf. Coat. Technol. 200 (2006) 4870–4875.
[26] M. Srivastava, V.K.W. Grips, K.S. Rajam, J. Appl. Electrochem. 38 (5) (2008) 669–677.
[27] L. Shi, C. Sun, P. Gao, F. Zhou, W. Liu, Appl. Surf. Sci. 252 (2006) 3591–3599.
[28] M. Srivastava, V.K.W. Grips, A. Jain, K.S. Rajam, Surf. Coat. Technol. 202 (2007) 310–318.
[29] M. Srivastava, V.K.W. Grips, K.S. Rajam, Appl. Surf. Sci. 253 (2007) 3814–3824.
[30] G. Wu, N. Li, D.L. Wang, D.R. Zhou, B.Q. Xu, K. Mitsuo, Mater. Chem. Phys. 87 (2004) 411–419.
[31] G. Wu, N. Lia, D. Zhou, K. Mitsuo, Surf. Coat. Technol. 176 (2004) 157–164.
[32] M. Pushpavanam, H. Manikandan, K. Ramanathan, Surf. Coat. Technol. 201 (2007) 6372–6379.
[33] L. Shi, C. Sun, W. Liu, Appl. Surf. Sci. 254 (2008) 6880–6885.
[34] G. Wu, N. Li, C.S. Dai, D.R. Zhou, Mater. Chem. Phys. 83 (2004) 307–314.
[35] S. Pané, E. Gmez, E. Vallés, J. Electroanal. Chem. 615 (2008) 117–123.
[36] M. Srivastava, V.K.W. Grips, K.S. Rajam, J. Alloys Compd. 469 (2009) 362–365.
[37] B. Bahadormanesh, A. Dolati, J. Alloys Compd. 504 (2010) 514–518.
[38] N. Guglielmi, J. Electrochem. Soc. 119 (1972) 1009–1012.
[39] C.T.J. Low, R.G.A. Wills, F.C. Walsh, Surf. Coat. Technol. 201 (2006) 371–383.
[40] A.F. Zimmerman, G. Palumbo, K.T. Aust, U. Erb, Mater. Sci. Eng. A 328 (2002) 137–146.
[41] A. Dolati, S. Mahshid, Mater. Chem. Phys. 108 (2008) 391–396.
[42] S.W. Watson, R.P. Walters, J. Electrochem. Soc. 138 (1991) 3633–3637.
[43] S.W. Watson, J. Electrochem. Soc. 140 (1993) 2235–2238.
[44] A.L. Morales, E.J. Podlaha, J. Electrochem. Soc. 151 (2004) 478–483.
[45] X. Cui, W. Wei, H. Liu, W. Chen, Electrochim. Acta 54 (2008) 415–420.
[46] H. Pelletier, J. Krier, P. Mille, Mech. Mater. 38 (2006) 1182–1198.
[47] A.C. Fischer-Cripps, P. Karvankova, S. Veprek, Surf. Coat. Technol. 200 (2006) 5645–5654.
[48] A. Bund, D. Thiemig, Surf. Coat. Technol. 201 (2007) 7092–7099.
[49] L. Benea, P.-L. Bonora, A. Borello, S. Martelli, Mater. Corros. 53 (2002) 23–29.
[50] Q. Feng, T. Li, H. Teng, X. Zhang, Y. Zhang, C. Liu, J. Jin, Surf. Coat. Technol. 202 (2008) 4137–4144.
[51] H.-Y. Zheng, M.-Z. An, J. Alloys Compd. 459 (2008) 548–552.